

www.acsami.org Research Article

Strain-Tunable Microfluidic Devices with Crack and Wrinkle Microvalves for Microsphere Screening and Fluidic Logic Gates

Ying Liu,[§] Min Cheng,[§] Jielong Huang, Yangchengyi Liu, Yao Chen, Yang Xiao, Shangda Chen, Xiaoping Ouyang, Huanyu Cheng,* and Xiufeng Wang*



Cite This: ACS Appl. Mater. Interfaces 2021, 13, 36849–36858



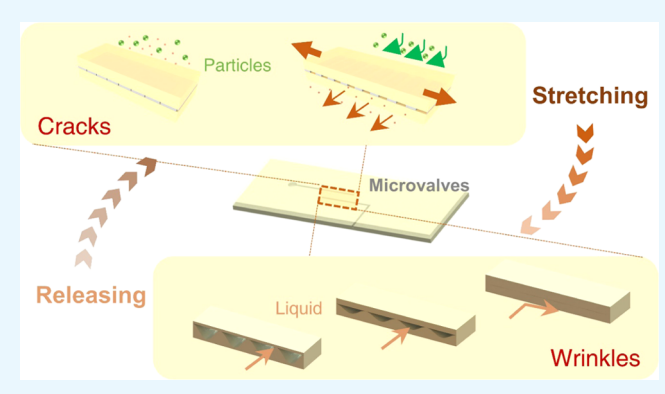
ACCESS

Metrics & More



Supporting Information

ABSTRACT: Mechanical instabilities in soft materials have led to the formation of unique surface patterns such as wrinkles and cracks for a wide range of applications that are related to surface morphologies and their dynamic tuning. Here, we report a simple yet effective strategy to fabricate strain-tunable crack and wrinkle microvalves with dimensions responding to the applied tensile strain. The crack microvalves initially closed before stretching are opened as the tensile strain is applied, whereas the wrinkle microvalves exhibit the opposite trend. Next, the performance of crack and wrinkle microvalves is characterized. The design predictions on the bursting pressure of microvalves and others from the theory agree reasonably well with the experimental measurements. The microfluidic devices with strain-tunable crack



and wrinkle microvalves have then been demonstrated for microsphere screening and programmable microfluidic logic devices. The demonstrated microfluidic devices complement the prior studies to open up opportunities in microparticle/cell manipulations, fluidic operations, and biomedicine.

KEYWORDS: cracks and wrinkles, microvalves, strain-actuated, microsphere screening, microfluidic logic gates

1. INTRODUCTION

With paramount importance in controlling fluid flow and handling microparticles, microfluidic devices can be applied to particle/cell manipulations, pharmaceuticals, and biomedicine. 1-4 Although the active control of particles can be achieved with various approaches (e.g., acoustics, electrophoreses,⁶ optical power,⁷ and microvalves^{8,9}), microvalve systems are capable of precise control of both particles and flows. The control in terms of on/off or speed of the particle/ flow in the device is often caused by the change in the geometry of microfluidic channels resulting from the phase transition of materials (e.g., hydrogel, 10 thermoreversible gelation polymers, 11 and shape-memory polymers 8). However, valves regulated by responsive materials are associated with long response times. While the microvalve can also be controlled by an external electromagnetic device, the use of external electromagnetic devices often results in complex devices, which is challenging in miniaturization and further integration.¹² Therefore, it remains a challenge to design and fabricate integrated microfluidic systems with active controls.

Because mechanical deformations (e.g., stretching) of the microfluidic device can modulate the channel dimension by separating particles or controlling the fluid flow, ^{13–15} the development of stretchable microfluidic technology has started gaining momentum in recent years. ¹⁶ With the strain-

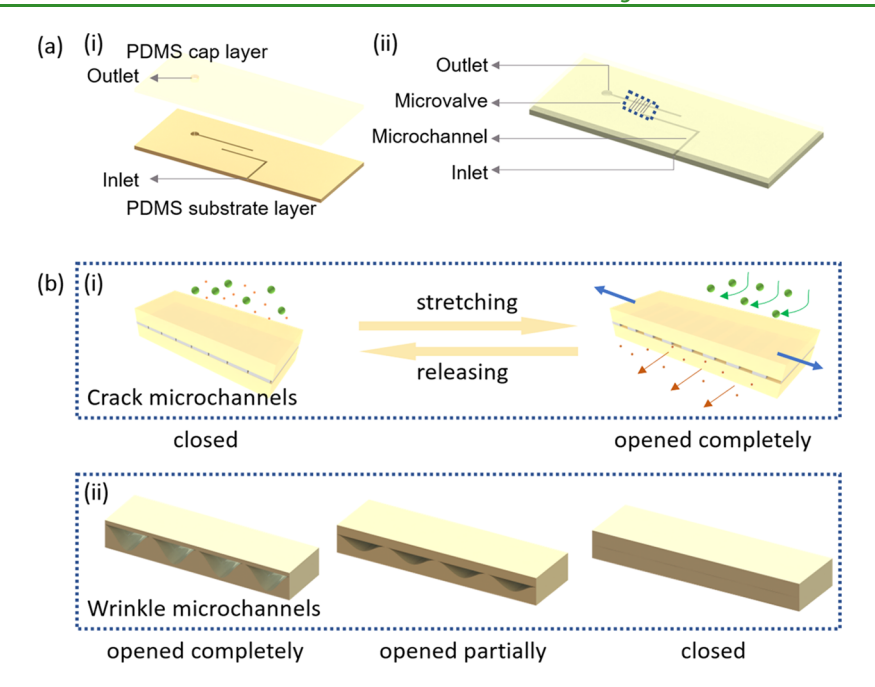
controlled alteration of interobstacle distances, deterministic lateral displacement devices can achieve tunable particle separation. ¹³ Mechanically actuated elastic deformations have also been utilized to control and direct fluid flow in a flexible microfluidic device with a bucked arch that can close the gap upon mechanical deformations, ¹⁴ but the application is limited by the large dimension (~millimeters) of the channel. Furthermore, an inertial microfluidic device with a tunable channel length upon stretching has been explored to modulate the force on particles of different sizes, which changes their flow rate ratios and separates particles. ¹⁵ Although various tunable functions have been demonstrated in the above stretchable microfluidic devices, it is still challenging to dynamically tune the bursting pressure of the microchannel as valves.

Because of instability and modulus mismatch, ^{17,18} wrinkles and cracks with micropatterns often appear on the surface of soft materials, including ruptured paint on the wall, wrinkled

Received: May 11, 2021 Accepted: July 19, 2021 Published: July 28, 2021







www.acsami.org

Figure 1. Schematic illustration of the strain-tunable microfluidic device for microsphere screening and fluidic logic gates. (a) Exploded schematic illustration describes the structure of the device. (b) Application of the microfluidic device (i) with strain-tunable active control to switch between the open and closed states for microparticle screening and (ii) the morphology changes of the wrinkle microvalves.

skin on the human body, and recently emerged stretchable electronics. 19-21 Compared to the methods based on thermal expansion, ²² swelling, ²³ and the use of focused ion beam, ²⁴ the combination of prestretching and ultraviolet/ozone (UVO) treatment can easily and controllably create parallel microstructures. In particular, controlled cracking has been applied as an alternative patterning tool to fabricate transparent conductors, ^{25,26} functional sensors, ^{27,28} crack lithography, ²⁹ three-dimensional (3D) structures, ³⁰ and microfluidics. ^{31,32} The microfluidic devices integrated with micropatterns can be used for protein enrichment, particle screening, DNA manipulation, and water management, 32-34 which show the feasibility of crack/wrinkle patterns as microchannels. However, their use as microvalves to dynamically adjust and control the fluid pressure, along with their combination for logic operation, is yet to be demonstrated. Without the use of expensive equipment and complicated processes, this potential simple and cost-effective method could compare favorably over with the alternative methods to prepare the microvalves (e.g., photolithography,^{35,36} boring a hole,³⁷ and electromagnettriggered method³⁸).

In this paper, we present a simple, cost-effective method to fabricate a stretchable microfluidic device based on a poly(dimethylsiloxane) (PDMS) layer with active controls enabled by arrays of tunable and reversible micropatterns. The micropatterns such as cracks and wrinkles have been easily prepared by a combination of a stretching strategy and the formation of a relatively stiff surface PDMS layer from ultraviolet/ozone (UVO) exposure. Stretching the PDMS with a stiff surface layer leads to crack microchannels, whereas the release of the prestrained PDMS with a stiff surface layer results in wrinkle microchannels. Both microchannels can be switched between the "on" and "off" states to serve as a microvalve by the applied tensile strain. The former is "off" in the unstretched state but "on" in the stretched state, whereas it is the opposite in the latter. When the microvalve is "on", its size can also be tunable by the level of tensile strains. The

application of tunable and reversible microchannels has been highlighted through microsphere screening and microfluidic logic gates.

2. RESULTS AND DISCUSSION

2.1. Design of Tunable Micropatterns in Microfluidic **Devices for Active Control.** The microfluidic device with active control consists of a top PDMS cap layer with an outlet and a bottom PDMS substrate that includes a connection to the inlet, two parallel microfluidic channels, and strain-tunable micropatterns (i.e., cracks or wrinkles) as microvalves (Figure 1). In a proof-of-concept embodiment, the device with a thickness of 1.2 mm is designed into a rectangular shape with a length of 3 cm and a width of 1.2 cm for a minimized overall footprint. The micropatterns are prepared by a combination of the stretching strategy and formation of a stiff PDMS surface layer (Figures S1 and S2). The thin, stiff PDMS surface layer of SiO_x is generated by UVO treatment of the selective PDMS substrate region for a time of up to 40 min under ambient conditions. After the formation of the stiff SiO_x layer on PDMS, applying tensile strain results in tunnel cracks as microvalves on the top layer. Although stress concentration occurs at the end of the microfluidic channel upon uniaxial stretching, the simulation results indicate a relatively uniform stress distribution in the region where crack microvalves are to be created (Figure S3). As a result, stretching along the microchannel direction successfully generates uniform crack microstructures in the brittle top SiO_x layer along the perpendicular direction in the experiment (Figure S3b). To prepare for wrinkle microvalves, the PDMS substrate is prestretched first, followed by UVO treatment of the selective region to generate a strain-free stiff SiO_x layer on the PDMS surface. The release of the prestrain allows the stiff SiO_x surface layer to form a sinusoidal wrinkled pattern on the soft PDMS substrate because of the uniaxial compressive stress. In addition to the 300 μ m-thick top PDMS cap layer with an outlet (diameter of 1.5 mm), the bottom PDMS substrate layer

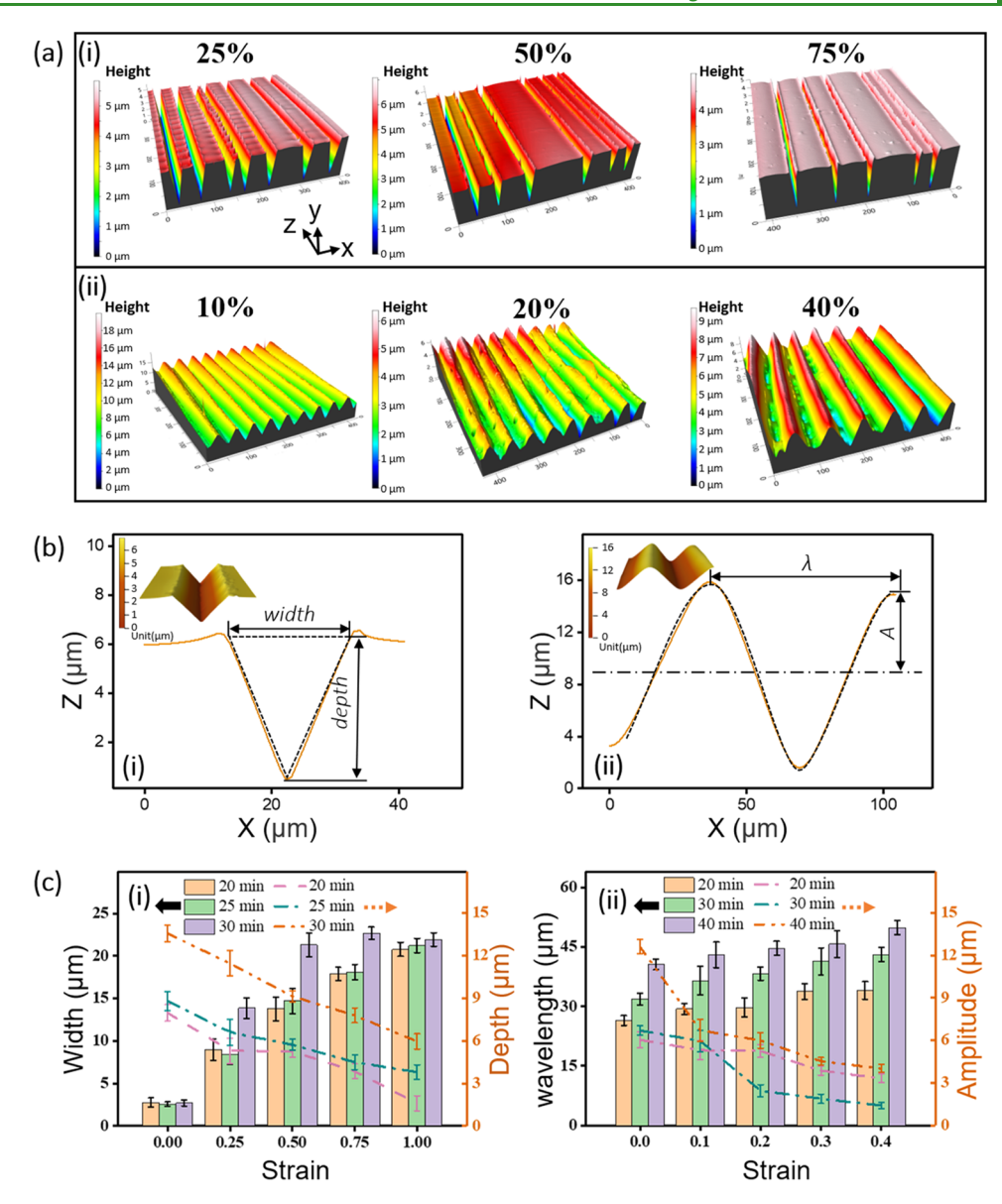


Figure 2. Characterization of microcracks and wrinkles. (a) 3D optical images of (i) microcracks and (ii) wrinkles for various tensile strain levels. (b) 3D optical images of the vertical line cut profile to show the cross-section of (i) microcracks with the triangular shape for a tensile strain of 25% and (ii) wrinkle with the sinusoidal shape before stretching. (c) Effects of the applied tensile strain and UVO treatment time on the cross-sectional profile: (i) width and depth of the microcracks and (ii) wavelength and amplitude of the wrinkles. The left bar chart is for the width/wavelength and the right dot—dash line is for the depth/amplitude.

with a thickness of 900 μ m includes two parallel microfluidic channels (300 μ m in width and height) and (crack or wrinkle) the microvalves generated between them. The ideal microvalve should also exhibit the characteristics of low leakage, low power consumption, fast speed, wide linear range, and wide adaptability for controlling the closed and open states of the microchannel. Because of the strain-tunable microvalves, the microfluidic device can be applied for microparticle screening and fluidic logic gates (Figure 1b).

2.2. Characterization of Microcracks and Wrinkles. Although the microcracks are considered as closed in the unstretched state (width of ca. 2.8 μ m), they gradually open as the tensile strain is increased from 25 to 50% and then to 75%, as indicated in their 3D optical images for a UVO treatment of 20 min (Figure 2a-i). The formation of microcracks in terms of width, depth, and average crack spacing can be reproducibly controlled by the UVO treatment time and strain (Figure S4).

Because the initial crack depth increases with the increasing thickness of the stiff SiO_x layer via UVO treatment, the thicker stiff layer from a longer UVO treatment leads to a larger initial crack depth. The relatively small error bars from at least 10 measurements indicate a reasonably high uniformity. Although a small variation exists, the reasonably high control in the formed crack microvalves has been demonstrated to be sufficient for flow rate and particular screening in this work. As the microcrack is stretched from 0 to 75%, its width increases from 2.8 to 20.8 μ m, whereas its depth decreases from 5.8 to 3.8 μ m. Before the top PDMS cap layer is applied, the cross-section of the microcrack can be approximately taken as a triangular shape. For a tensile strain of 25%, the 3D optical image indicates that the microcrack exhibits a depth of 5.5 μ m and a width of 20 μ m (Figure 2b-i). The cracks on the surface are relatively uniform, as evidenced by the cross-sectional shapes with an average crack width of 5.06 μ m and a variance

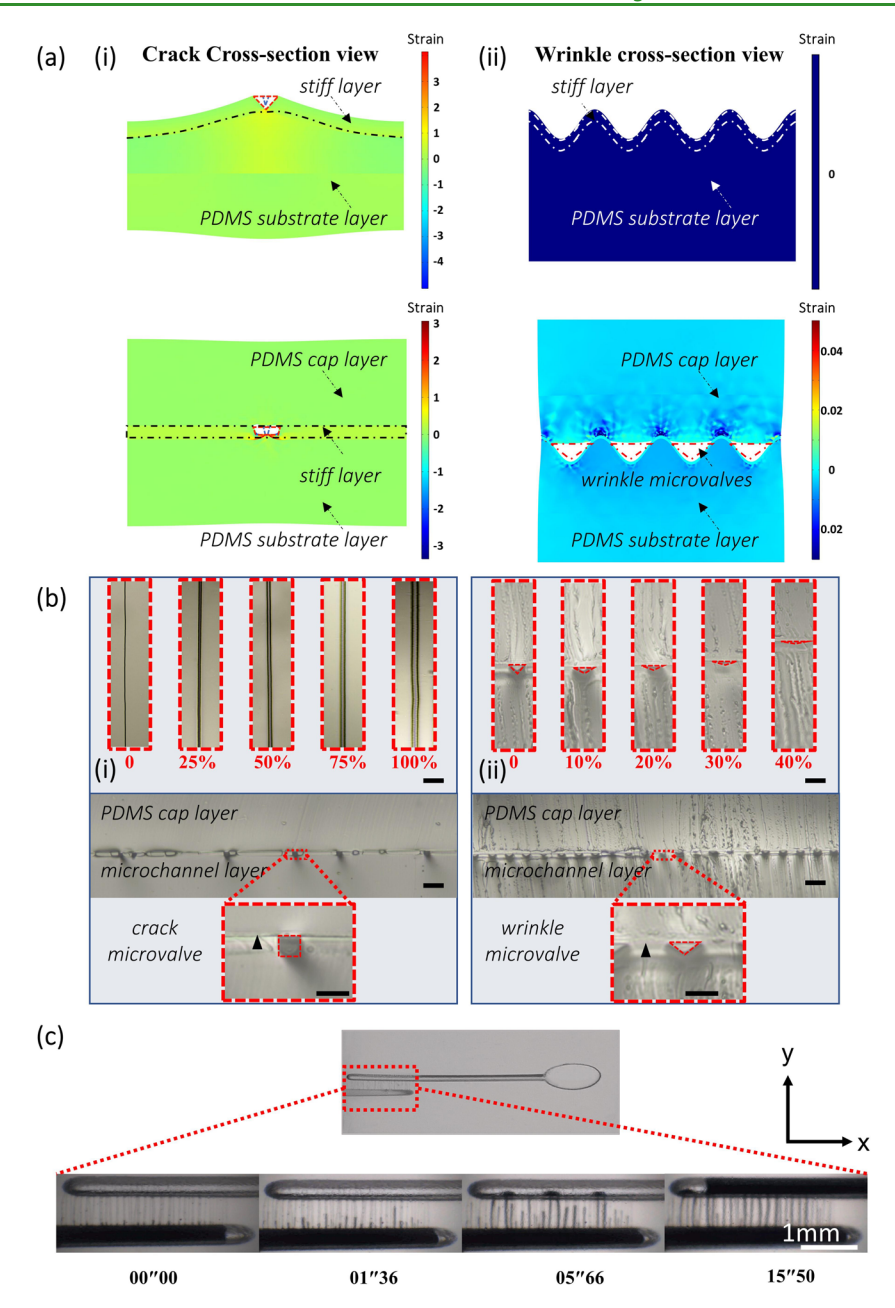


Figure 3. Performance evaluation of the crack and wrinkle microvalves. (a) Deformation and strain distribution of the crack microvalves and wrinkle microvalves before and after the use of the soft PDMS cap layer (Young's modulus of 130 GPa for the stiff SiO, layer and 1.8 MPa for the soft PDMS¹⁸). (b) Optical images to show (i) the crack microvalves (at a tensile strain of 0, 25, 50, 75, and 100%) and (ii) wrinkle microvalves (at a tensile strain of 0, 10, 20, 30, and 40%). Black triangles indicate the interface between the top and the bottom PDMS layer, whereas the red dotted lines indicate the microvalves. Scale bar: 50 µm (inset: 10 µm). (c) Optical images to show the liquid flow sequence in the crack microvalves. Scale bar: 1 mm.

of 0.56 (Figure S7a). In the cyclic test between 0 and 100% tensile strain at a frequency of 2 Hz for 20 cycles, the cracks repeatedly form to indicate the robustness of the method, although few new cracks may appear due to slight variations in the experiment (e.g., loading rate and tensile strain) (Figure S6). Although the width of microcracks significantly increases with the tensile strain for a given UVO treatment time (Figure 2c-i), the device easily breaks once the applied strain exceeds the initial prestrain of 100% due to the stress concentration at the end of the microfluidic channel. Therefore, the tensile strain of 100% is chosen as the maximum value. Because the increased UVO treatment time increases the thickness of the SiO_x surface layer, ^{39,40} both the width and depth of the

microcracks increase with the treatment time in a wellcontrolled manner. Although the width of microcracks increases with the treatment time, the value saturates, especially when the applied tensile strain is large. The initial crack density decreases as the UVO treatment time increases (Figure S5c). For instance, the width of the microcrack increases from 20.8 to 21.9 μm by only 5% as the UVO treatment time increases from 20 to 30 min for an applied tensile strain of 100%. Therefore, the UVO treatment of 20 min is used in the following experiments for ease of fabrication unless otherwise specified. Furthermore, the width of the formed cracks can be easily controlled by the applied strain to the open and closed states.

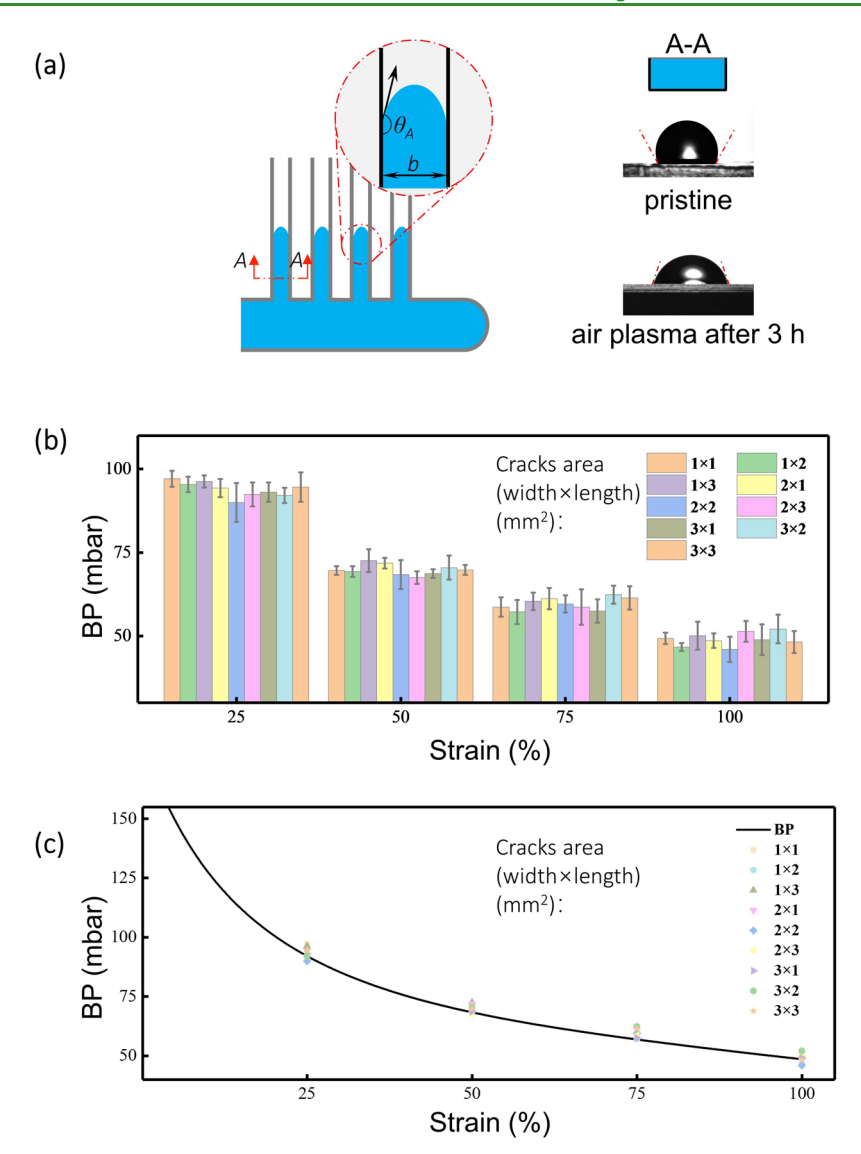


Figure 4. Characterization of bursting pressure (BP) of the microvalve. (a) Schematic showing the burst valve with contact angles of the pristine PDMS and that after UVO exposure for 20 min. After UVO exposure of PDMS for 20 min, its water contact angle reduces from 109 to 95° . (b) Measured BP as a function of the applied tensile strain from 25 to 100% in the array of crack microvalves with different cracked areas (width \times length). (c) Comparison of BP versus tensile strain between the theory (black line) and the experimental result (symbols).

Compared to the microcracks, the microwrinkles exhibit an even higher uniformity. As the microwrinkles are stretched from 10 to 20% and then to 40% for a UVO treatment of 40 min, the wavelength of the wrinkles increases from 40.6 to 44.6 and then to 49.8 μ m, whereas the depth decreases from 12.6 to 6.0 and then to 4.0 μ m (Figure 2a-ii). Different from the triangular shape in the microcracks, the cross-section of the microwrinkle is approximately a sinusoidal shape with a wavelength of 60 μ m and an amplitude of 7.1 μ m before stretching (Figure 2b-ii). As the applied tensile strain is increased, the amplitude decreases, whereas the wavelength increases, as indicated in the 3D optical images (Figures 2c-ii and S7b).

2.3. Performance of the Crack/Wrinkle Microchannels in the Microfluidic System. Although the prepared microcracks and wrinkles exhibit triangular and sinusoidal shapes, applying a soft PDMS cap layer on the two micropatterns could drastically change the cross-sectional shapes of the resulting crack and wrinkle microvalves. The effect of the cap layer on the resulting crack and wrinkle

microvalves is first studied in the microvalve systems with and without the cap layer by finite element analysis (Figure 3a). When the PDMS samples are thermocured for more than 10 h, there is no significant change in PDMS elasticity within 5 months. 41 The demonstrated application in this study is within 5 months after the structure is generated with the PDMS samples thermocured for over 10 h. Although there might be a time-dependent variation in PDMS elasticity over time, the PDMS elasticity is mostly concerned when we initially generate the crack and wrinkle microstructures. The open and closed states of the resulting microvalves are controlled by the applied tensile strain, which has little to do with the slight change in PDMS elasticity. The soft PDMS cap layer changes the crosssectional shape of crack microvalves from a triangular to a rectangular-like shape for a tensile strain of 25%, whereas wrinkle microvalves are changed from a sinusoidal to a triangular shape. The prediction of changes in the crosssectional shapes from the simulation is verified by the experimental results as different tensile strains are applied to the array of crack microvalves (Figure 3b-i). The soft PDMS cap layer also changes the cross-sectional shape from sinusoidal to triangular in wrinkle microvalves (Figure 3b-ii). Compared to the initial wavelength and amplitude of the sinusoidal wrinkles, the width and depth of the triangular shape also reduce by 69% because of the interaction between the top cap layer and the wrinkles. As the tensile strain increases, the crosssectional area of the triangular shape further decreases, suggesting a feasible yet simple strain-tunable approach for the active control of microvalves. The spacing of 101 μ m with a variance of 8.8 µm between cracks before stretching slightly increases as the tensile strain increases (Figure S8b). The performance of the crack microvalves is then demonstrated to modulate the liquid flow between two parallel microchannels over time (Figure 3c). A pressure of 150 mbar is applied to ensure liquid flow from the microfluidic channel (connected to the inlet) to the other microchannel (connected to the outlet) through crack microvalves at a tensile strain of 50%. As the time starts to elapse from the beginning to 1"36, almost half of the microvalves in the array begin to show liquid flow. Liquid flow occurs in most of the microvalves and reaches the other microchannel through half of the microvalves at 5"66. The liquid completely passes through the crack microvalves at 15"50. It should be noted that there is variation among the generated crack microvalves in the array. Although this variation affects the speed of the liquid flow, all of the crack microvalves can be switched open to allow for liquid flow within a short period of time (Figure 3c).

Because of the width deviation in the microvalves, the flow speed is not the same in every microvalve (Figure 4a). The crack and wrinkle microvalves with a significantly reduced width (i.e., ca. 15 times compared to the microchannel) work as burst valves to control the fluid flow (Figure 4b). When the applied pressure is lower than the characteristic bursting pressures (BPs), the microvalves remain closed, as the surface tension between the fluid and the microvalve channel wall is not sufficient to drive the fluid flow. Cracks exist in the microfluidic system, even after the strain has been completely removed. Due to the presence of surface forces, they could vanish after a period of healing time. 42 Although the width and depth of cracks are not zero at 0% applied strain, the estimated BP of 183 mbar is sufficiently high to maintain the closed state for microvalves. Although the surface tension in the microvalve can be modulated, it is easy to use an external microinjection pump to provide the elevated pressure at a step size of 5 mbar for driving the fluid flow. As the performance of the capillary burst valve is characterized by the bursting pressure, the burst pressure values for the array of microvalves with different crack areas (width × length) at various tensile strains are investigated. The pressure value that initiates the flow experimentally measures the bursting pressure. The bursting pressure is observed to decrease with the increasing tensile strain that increases the width of the crack. Meanwhile, the BPs are not statistically different among those arrays with different crack lengths and numbers of the cracks. The selective area where the cracks generated (from $1 \times 1 \text{ mm}^2$ to $3 \times 3 \text{ mm}^2$) is small compared to the entire device $(3 \times 1.2 \text{ cm}^2)$. When uniaxial stretching is applied, the strain distribution in the treated area is uniformly formed (Figure S3a) and then the cracks for microvalves with the same BP are produced.

The Young-Laplace equation also relates the BP in a rectangular microvalve with a width of b and depth of h to the surface tension σ of the liquid as 36,43

$$BP = -2\sigma \left[\frac{\cos \theta_{A}}{b} + \frac{\cos \theta_{B}}{h} \right] \tag{1}$$

where θ_{A} (θ_{B}) is the contact angle at the sidewall/bottom (or top) surfaces of the microvalve. The sidewall of the channel has the same contact angle ($109 \pm 0.2^{\circ}$) as the intrinsic bottom PDMS surface, as the cracks are generated after finishing the UVO treatment. After 5 min of "high" power plasma treatment of the top surface, its contact angle initially decreases to a significantly smaller value and then saturates to $78 \pm 0.5^{\circ}$ after 3 h of recovery (Figure S9). Although Poisson's effect would induce wrinkles in the direction perpendicular to the stretching direction, the induced wrinkles become negligibly small after applying the cap layer (Figure \$10). The cap layer also affects the changes in the cross-sectional area, width, and depth of the crack as a function of the tensile strain (Figure S11). The crack width changes with the tensile strain (ε) to follow the fitting function of $b = 14.456\varepsilon + 2.608$ $(R^2 = 0.99)$, whereas the crack depth follows the fitting function of $h = 2.904\epsilon^2 - 4.276\epsilon + 5.326$ ($R^2 = 0.94$). As a result, the BP in eq 1 becomes

$$BP = -\sigma \left[\frac{2\cos\theta_{A}}{14.456\varepsilon + 2.608} + \frac{\cos\theta_{A}}{2.904\varepsilon^{2} - 4.28\varepsilon + 5.32602} + \frac{\cos\theta_{B}}{2.904\varepsilon^{2} - 4.28\varepsilon + 5.326} \right]$$
(2)

which decreases as the tensile strain increases (Figure 4c). The theoretical predictions show reasonable agreements with the experimental results. The difference between experimental measurements and the theory is likely attributed to the nonstraight microvalves. Flow rate is another important parameter to characterize the performance of the microvalve. Since an applied pressure of 150 mbar is sufficient to burst open the microvalves for fluid flow, the pressure up to 150 mbar is applied to different crack microvalve arrays with different cracked areas (width × length) for the measurement of flow rate (Figure S12). Because the hydraulic resistance to fluid flow of a rectangular microchannel with a high aspect ratio follows $R = 12\mu L/(wh^3)$, ⁴⁴ the increase in the crosssectional dimensions can decrease hydraulic resistance. Therefore, the changes in the geometry and dimension of the microvalves from mechanical deformations (e.g., stretching) can easily modulate the hydraulic resistance and flow rate. The flow rate monotonically increases from 0.04 to 0.34 mm³/s as the tensile strain increases from 25 to 100%. The slower fluid flow is also observed in the longer and narrower crack areas because the former takes a longer time and the latter results in a smaller number of crack microvalves. The flow control by the tensile strain applied to the microvalves represents another important tunable parameter of microfluidic platforms for biomedical research and clinical diagnosis.

2.4. Applications of Microvalves for Microsphere Screening and Fluidic Logic Gates. As a proof-of-concept demonstration, the strain-tunable microvalves are first applied to screen polydisperse microspheres based on their sizes. An airtight tube connects the microfluidic device to the pressure pump. The microsphere suspension consists of two types of microspheres, one with a small diameter of $D = 2 \mu m$ and the other with a large diameter of $D = 5 \mu m$. When the suspension

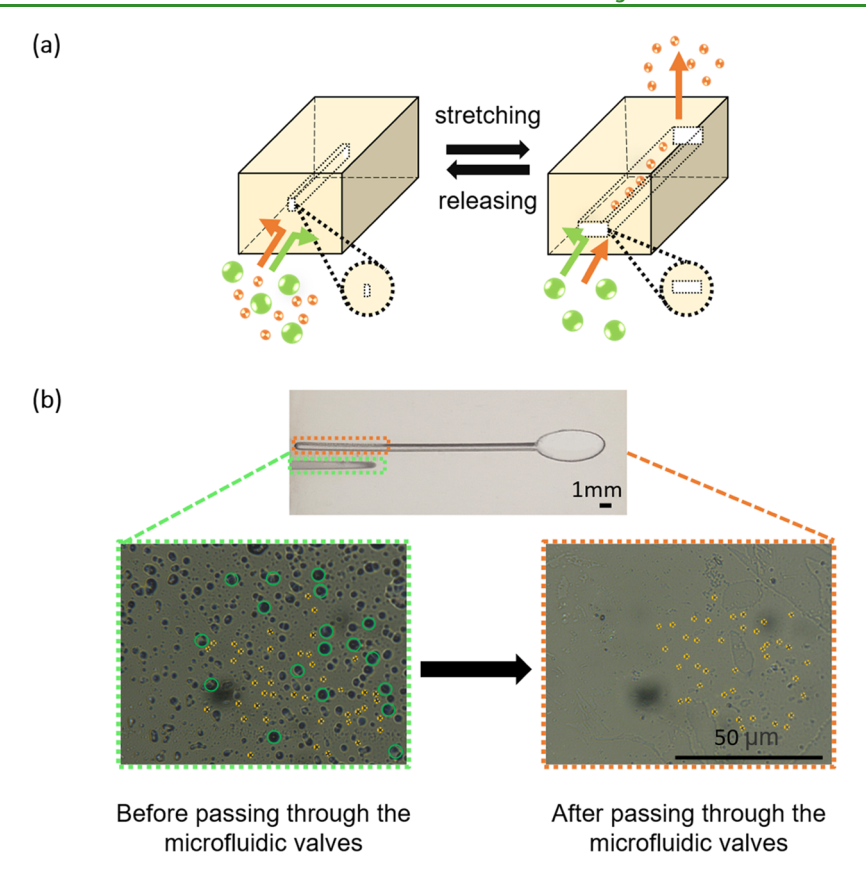


Figure 5. Strain-tunable microvalves for microsphere screening. (a) Schematic showing the working principle of the microfluidic microvalve that changes its width and depth to allow selective transport. (b) Optical images of the polydisperse mixture before (yellow dashed box) and after (green dashed box) it passes through the microfluidic valves for a tensile strain of 100%. Scale bars: 50 μ m.

is injected from the tube into the device at a pressure of 150 mbar, the crack microvalves remained closed to both microspheres, as the width of 2 μ m in the encapsulated crack microvalves is smaller than both types of microspheres before stretching (Figure 5a). When the applied strain is 100%, the width of the crack of 20.8 \pm 0.8 μ m becomes much larger than the depth of 1.6 \pm 0.5 μ m, so the depth controls the particle screening. As a result, the crack microvalves after 100% stretching allows the transport of the smaller microspheres (D = 2 μ m) while preventing the transport of the large particles $(D = 5 \mu m)$. The strain-tunable selective transport of the smaller microspheres is fairly effective, as confirmed by the polydisperse mixture in the two parallel microchannels (Figure 5b). The polydisperse mixture includes both large microspheres ($D = 5 \mu m$, circled in green) and small microspheres $(D = 2 \mu m, \text{ circled in yellow})$ before it passes through the microvalve, whereas the microfluidic channel after the microvalve only includes the small microspheres. The measured particle size distribution by counting from the microscopy images is shown in Figure S13. Considering the dimension change in the PDMS channel, particle screening can be applied for the particles in the range from 2 to 20 μ m, which is relevant to various types of cells. Changes in the tensile strain also allow the selective transport of particles/cells of other sizes.

As a proof-of-concept demonstration toward the future multiliquid, multistep sample preparation and reagent processing (e.g., biphasic liver analysis), the control of the liquid flow in a two-valve system is first investigated in this study. Because the crack and wrinkle microvalves switch

between the on and off states in an opposite trend upon stretching, they can be applied to develop a new class of fluidic "OR" logic gates (Figure 6). In the design of the OR gates, the microfluidic device has a shared inlet and two different outlets, with one connected to the wrinkle microvalve (i.e., type A) and the other connected to the crack microvalve (i.e., type B) (Figure 6a). With the target truth table (Figure 6b), both the crack and wrinkle microvalves are created between the two parallel microchannels (Figure 6c, black box). An input is considered as 1 (or 0) when the fluid flows from the inlet to the outlet, which is otherwise 0. The output is 1 if the fluid flows out from the outlet(s), which is otherwise 0. Without the fluid flow to the inlet (i.e., 0 for both A and B), there is no fluid flow out of any outlets, resulting in 0 in the outlet. When the fluid flows into the inlet of the microfluidic device with no stretching applied, the wrinkle microvalve is open, but the crack microvalve is closed (i.e., 1 for A and 0 for B) (Figure 6c). As the tensile strain is increased to 40%, the crack microvalve opens, but the wrinkle microvalve closes (i.e., 0 for A and 1 for B). Because the output is 1 for both of the above two cases (i.e., before or after the tensile strain of 40%), the OR logic gate is demonstrated. Furthermore, by changing the parallel connection of the crack and wrinkle microvalves to series, the OR logic gate becomes the "AND" logic gate. The design and demonstration of various fluidic logic gates provide the microfluidic devices with the capabilities to perform fluidic operations. This controllable valve represents a viable path toward large-scale integration for potential applications in multiliquid, multistep sample preparation and reagent processing (Figure 6d).

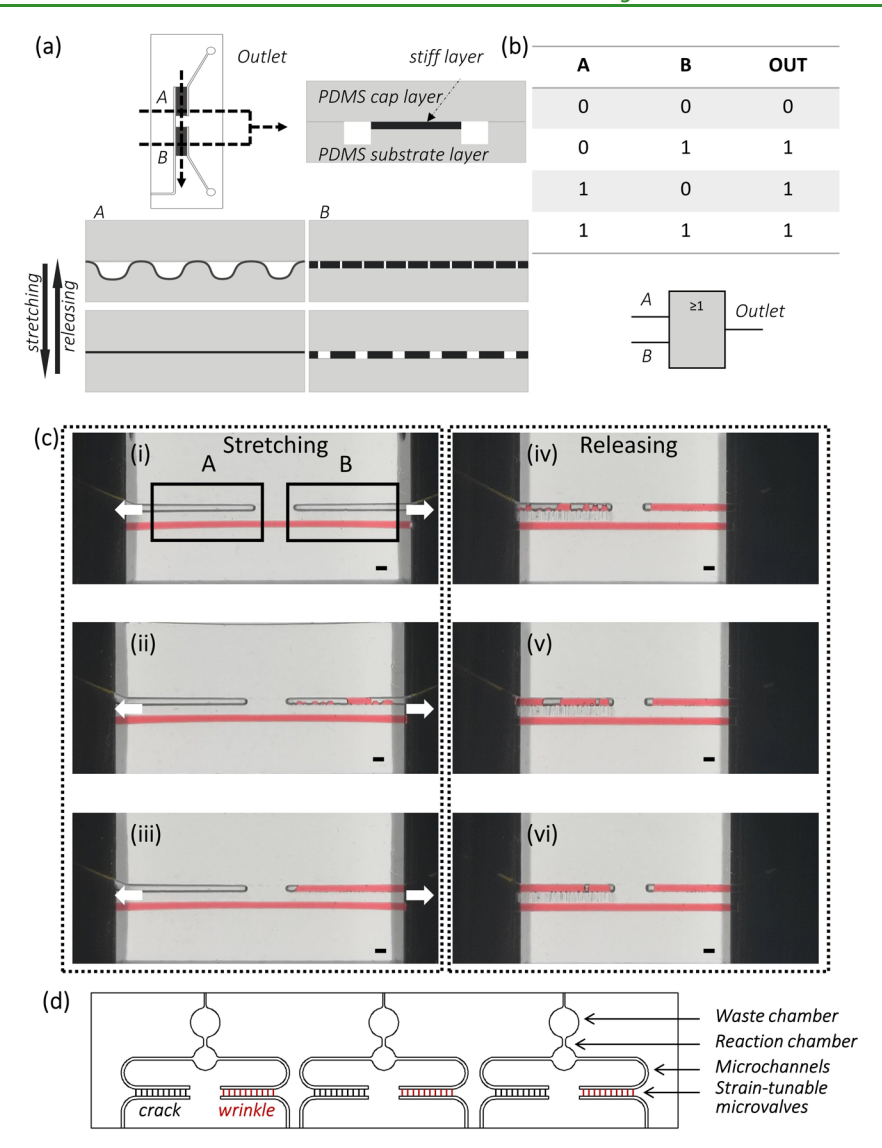


Figure 6. Demonstration of the microvalves as the fluidic logic gate. (a) Schematic to show the design of the microfluidic device with crack and wrinkle microvalves as the OR logic gate. (b) Fluidic OR logic gate and its corresponding truth table. (c) Optical images of the liquid flow to show the operation of the fluidic OR logic gate. (i–iii) Liquid flow sequence in the crack microvalves (box B, open) after 40% stretching and (iv–vi) the liquid flow in the wrinkle microvalves (box A, open) during a gradual releasing process. Scale bar: 1 mm. (d) Potential application in multiliquid, multistep sample preparation and reagent processing.

3. CONCLUSIONS

In summary, we report a simple yet effective approach to fabricate strain-tunable elastomeric micropatterns (e.g., cracks and wrinkles) as microvalves in a microfluidic device. The crack microvalves are closed before stretching but open as the tensile strain increases, whereas the wrinkle microvalves exhibit the opposite trend. The microfluidic device with crack and wrinkle microvalves is demonstrated for microparticle screening and fluidic logic operation in a programmable manner. The applied tensile strain changes the width and depth of the crack microvalves to control the selective transport of microparticles of different sizes. When the crack and wrinkle microvalves are integrated into the single microfluidic device, the fluid can be modulated to flow through the microvalves in a manner that represents the operation of the OR or AND logic gates. These controllable valves to adjust the reaction time and volume represent a viable path toward large-scale integration for potential applications in multiliquid, multistep sample preparation and reagent processing. The programmable

microfluidic system demonstrated in this study opens up additional opportunities to complement the prior reports in applications ranging from biomedicine and organ-on-chips to drug delivery and reagent mixing. However, PDMS is prone to swelling in many organic solvents. Although the application of the device with PDMS is limited (aqueous solutions), the concept from this study can be applied to the other soft materials that are stable in the target organic solvent.

4. EXPERIMENTAL SECTION

4.1. Preparation of the Microfluidic Device. Analytical grade chemicals were used as received. The PDMS precursors (SYLGARD 184, Dow Corning) and poly(styrene sulfonic acid) sodium salt (PSSNa, $M_{\rm w}=70\,000$ Da) were obtained from the Alfa Aesar Co., Inc. The PDMS base and curing agent were mixed at a weight ratio of 10:1. After degassing the PDMS prepolymer, it was cast onto a poly(methyl methacrylate) (PMMA) mold fabricated by a laser engraving machine (CNN, JK-DK40, Wenhao Co., Ltd., China). Curing at 70 °C for 12 h produced the PDMS mold with extruded microchannel features. Casting another PDMS precursor (weight

ratio of 10:1) on the PDMS mold was followed by curing at 70 °C for 12 h. Peeling off the cured PDMS with care resulted in the PDMS substrate with recessed channels that were replicated from the mold. With a shadow mask, the channel region of the cured PDMS substrate was selectively treated with UVO at a distance of 3.5 cm for 20 min in a bench-top UVO etcher (BZS250GF-TX, HWOTECH Science and Technology Ltd., China). After the PDMS substrate was stretched to a tensile strain of 100% for 10 s by a custom-built stretcher (Figure S14), an array of microscale cracks were created as microvalves. The uniaxial tensile strain was measured by a digital caliper with a resolution of 0.01 mm. After air plasma treatment (Harrick Plasma Cleaner, PDC-002-HP, Harrick Plasma) with high power for 5 min, bonding another PDMS cap layer on the PDMS substrate with microfluidic channels and valves completed the fabrication.

- **4.2. Structural Characterizations.** The dimensions of the microscale crack (e.g., width, depth, and spacing) and surface profiles of the micropatterns were determined by a Profilm 3D optical profilometer (Filmetric Inc.). The surface morphology of the PDMS substrate under various applied strains was collected by an optical microscope (PH100, Phenix, China). Sessile water droplet contact angles (CAs) were acquired using a model 250 (p/n 250-F1) optical contact angle meter (rame-hart) at an ambient temperature of 25 °C. After applying 5 μL of deionized water on the samples by an automatic dispense controller, the CAs were automatically determined from the Laplace—Young equation.
- **4.3. Microsphere Screening.** The ${\rm SiO}_2$ particles (Luo Chuang Chemical, China) in the water were injected into the microchannel of the microfluidic device by a syringe pump. The particle migration in the microchannel was observed by an optical microscope (VHX-2000C, KEYENCE, Japan). The focusing location of particles was analyzed using Phmias.
- **4.4. Microfluidic Logic Device.** According to the presence or absence of fluid flow in the channel, the Boolean number of 0 or 1 was assigned to the corresponding channel. When the fluid appeared in the A or B area, the logic value of 1 was assigned to the wrinkle or crack microvalves. The fluid existence in the area was determined by the channel deformation induced by mechanical stretching.

ASSOCIATED CONTENT

Supporting Information

The Supporting Information is available free of charge at https://pubs.acs.org/doi/10.1021/acsami.1c08745.

Fabrication processes; the influence of processing parameters and strain levels, and encapsulation; morphology and flow rate; particle size distribution; and experimental setup (PDF)

AUTHOR INFORMATION

Corresponding Authors

Huanyu Cheng — Department of Engineering Science and Mechanics, The Pennsylvania State University, University Park, Pennsylvania 16802, United States; ● orcid.org/0000-0001-6075-4208; Email: Huanyu.Cheng@psu.edu

Xiufeng Wang — School of Materials Science and Engineering, Xiangtan University, Xiangtan 411105 Hunan, China; orcid.org/0000-0002-9557-049X; Email: onexf@xtu.edu.cn

Authors

Ying Liu — School of Materials Science and Engineering, Xiangtan University, Xiangtan 411105 Hunan, China Min Cheng — School of Materials Science and Engineering, Xiangtan University, Xiangtan 411105 Hunan, China Jielong Huang — School of Materials Science and Engineering, Xiangtan University, Xiangtan 411105 Hunan, China Yangchengyi Liu — School of Materials Science and Engineering, Xiangtan University, Xiangtan 411105 Hunan, China

Yao Chen – School of Materials Science and Engineering, Xiangtan University, Xiangtan 411105 Hunan, China

Yang Xiao – School of Materials Science and Engineering, Xiangtan University, Xiangtan 411105 Hunan, China

Shangda Chen – School of Materials Science and Engineering, Xiangtan University, Xiangtan 411105 Hunan, China

Xiaoping Ouyang – School of Materials Science and Engineering, Xiangtan University, Xiangtan 411105 Hunan, China

Complete contact information is available at: https://pubs.acs.org/10.1021/acsami.1c08745

Author Contributions

§Ying Liu and Min Cheng contributed equally to this work.

Notes

The authors declare no competing financial interest. One or more provisional patents are being filed on this work.

ACKNOWLEDGMENTS

This research was supported by the National Natural Science Foundation of China (11872326), Natural Science Foundation of Hunan Province (2018JJ2379 and 2018JJ2396), Scientific Research Fund (18B089) of Hunan Provincial Education Department, and Open Fund from the Institute of Flexible Electronics Technology of THU (2019KF1102). H.C. would like to acknowledge the support from the National Science Foundation (NSF) (Grant No. ECCS-1933072), the Doctoral New Investigator grant from the American Chemical Society Petroleum Research Fund (59021-DNI7), the National Heart, Lung, and Blood Institute of the National Institutes of Health under Award Number R61HL154215, and Penn State University.

REFERENCES

- (1) Zhang, Y.; Chen, Y.; Huang, J.; Liu, Y.; Peng, J.; Chen, S.; Song, K.; Ouyang, X.; Cheng, H.; Wang, X. Skin-interfaced microfluidic devices with one-opening chambers and hydrophobic valves for sweat collection and analysis. *Lab Chip* **2020**, *20*, 2635–2645.
- (2) Kim, J. Y.; Ahn, S. W.; Lee, S. S.; Kim, J. M. Lateral migration and focusing of colloidal particles and DNA molecules under viscoelastic flow. *Lab Chip* **2012**, *12*, 2807–2814.
- (3) Lee, D. J.; Brenner, H.; Youn, J. R.; Song, Y. S. Multiplex Particle Focusing via Hydrodynamic Force in Viscoelastic Fluids. *Sci. Rep.* **2013**, *3*, No. 3258.
- (4) Cha, J.; Shin, H.; Kim, P. Crack/Fold Hybrid Structure-Based Fluidic Networks Inspired by the Epidermis of Desert Lizards. ACS Appl. Mater. Interfaces 2016, 8, 28418–28423.
- (5) Zheng, F.; Li, Y.; Hsu, H.-S.; Liu, C.; Tat Chiu, C.; Lee, C.; Ham Kim, H.; Shung, K. K. Acoustic trapping with a high frequency linear phased array. *Appl. Phys. Lett.* **2012**, *101*, No. 214104.
- (6) Kumar, A.; Kwon, J.-S.; Williams, S. J.; Green, N. G.; Yip, N. K.; Wereley, S. T. Optically Modulated Electrokinetic Manipulation and Concentration of Colloidal Particles near an Electrode Surface. *Langmuir* **2010**, *26*, 5262–5272.
- (7) Yang, A. H. J.; Moore, S. D.; Schmidt, B. S.; Klug, M.; Lipson, M.; Erickson, D. Optical manipulation of nanoparticles and biomolecules in sub-wavelength slot waveguides. *Nature* **2009**, *457*, 71–75.
- (8) Yang, S. H.; Park, J.; Youn, J. R.; Song, Y. S. Programmable microfluidic logic device fabricated with a shape memory polymer. *Lab Chip* **2018**, *18*, 2865–2872.

- (9) Sánchez-Ferrer, A.; Fischl, T.; Stubenrauch, M.; Albrecht, A.; Wurmus, H.; Hoffmann, M.; Finkelmann, H. Liquid-Crystalline Elastomer Microvalve for Microfluidics. *Adv. Mater.* **2011**, 23, 4526–4530.
- (10) Beebe, D. J.; Moore, J. S.; Bauer, J. M.; Yu, Q.; Liu, R. H.; Devadoss, C.; Jo, B.-H. Functional hydrogel structures for autonomous flow control inside microfluidic channels. *Nature* **2000**, 404, 588–590.
- (11) Ozaki, K.; Sugino, H.; Shirasaki, Y.; Aoki, T.; Arakawa, T.; Funatsu, T.; Shoji, S. Microfluidic cell sorter with flow switching triggered by a sol-gel transition of a thermo-reversible gelation polymer. *Sens. Actuators, B* **2010**, *150*, 449–455.
- (12) Rahbar, M.; Shannon, L.; Gray, B. L. Design, fabrication and characterization of an arrayable all-polymer microfluidic valve employing highly magnetic rare-earth composite polymer. *J. Micromech. Microeng.* **2016**, *26*, No. 055012.
- (13) Beech, J. P.; Tegenfeldt, J. O. Tuneable separation in elastomeric microfluidics devices. *Lab Chip* **2008**, *8*, 657–659.
- (14) Holmes, D. P.; Tavakol, B.; Froehlicher, G.; Stone, H. A. Control and manipulation of microfluidic flow via elastic deformations. *Soft Matter* **2013**, *9*, 7049–7053.
- (15) Fallahi, H.; Zhang, J.; Nicholls, J.; Phan, H.-P.; Nguyen, N.-T. Stretchable Inertial Microfluidic Device for Tunable Particle Separation. *Anal. Chem.* **2020**, *92*, 12473–12480.
- (16) Fallahi, H.; Zhang, J.; Phan, H.-P.; Nguyen, N.-T. Flexible Microfluidics: Fundamentals, Recent Developments, and Applications. *Micromachines* **2019**, *10*, 830–855.
- (17) Jiang, H.; Khang, D.-Y.; Song, J.; Sun, Y.; Huang, Y.; Rogers, J. A. Finite deformation mechanics in buckled thin films on compliant supports. *Proc. Natl. Acad. Sci. U.S.A.* **2007**, *104*, 15607–15612.
- (18) Li, Z.; Zhai, Y.; Wang, Y.; Wendland, G. M.; Yin, X.; Xiao, J. Harnessing Surface Wrinkling—Cracking Patterns for Tunable Optical Transmittance. *Adv. Opt. Mater.* **2017**, *5*, No. 1700425.
- (19) Zhou, H.; Zhang, Y.; Qiu, Y.; Wu, H.; Qin, W.; Liao, Y.; Yu, Q.; Cheng, H. Stretchable piezoelectric energy harvesters and self-powered sensors for wearable and implantable devices. *Biosens. Bioelectron.* **2020**, *168*, No. 112569.
- (20) Yi, N.; Shen, M.; Erdely, D.; Cheng, H. Stretchable gas sensors for detecting biomarkers from humans and exposed environments. *TrAC, Trends Anal. Chem.* **2020**, 133, No. 116085.
- (21) Yi, N.; Cui, H.; Zhang, L. G.; Cheng, H. Integration of biological systems with electronic-mechanical assemblies. *Acta Biomater.* **2019**, 95, 91–111.
- (22) Bowden, N.; Brittain, S.; Evans, A. G.; Hutchinson, J. W.; Whitesides, G. M. Spontaneous formation of ordered structures in thin films of metals supported on an elastomeric polymer. *Nature* **1998**, 393, 146–149.
- (23) Yang, S.; Khare, K.; Lin, P.-C. Harnessing Surface Wrinkle Patterns in Soft Matter. Adv. Funct. Mater. 2010, 20, 2550-2564.
- (24) Moon, M.-W.; Lee, S. H.; Sun, J.-Y.; Oh, K. H.; Vaziri, A.; Hutchinson, J. W. Wrinkled hard skins on polymers created by focused ion beam. *Proc. Natl. Acad. Sci. U.S.A.* **2007**, *104*, 1130–1133.
- (25) Han, Y.; Lin, J.; Liu, Y.; Fu, H.; Ma, Y.; Jin, P.; Tan, J. Crackle template based metallic mesh with highly homogeneous light transmission for high-performance transparent EMI shielding. *Sci. Rep.* **2016**, *6*, No. 25601.
- (26) Gupta, R.; Rao, K. D. M.; Srivastava, K.; Kumar, A.; Kiruthika, S.; Kulkarni, G. U. Spray Coating of Crack Templates for the Fabrication of Transparent Conductors and Heaters on Flat and Curved Surfaces. ACS Appl. Mater. Interfaces 2014, 6, 13688–13696.
- (27) Park, B.; Lee, S.; Choi, H.; Kim, J. U.; Hong, H.; Jeong, C.; Kang, D.; Kim, T.-i. A semi-permanent and durable nanoscale-crack-based sensor by on-demand healing. *Nanoscale* **2018**, *10*, 4354–4360.
- (28) Sun, H.; Dai, K.; Zhai, W.; Zhou, Y.; Li, J.; Zheng, G.; Li, B.; Liu, C.; Shen, C. A Highly Sensitive and Stretchable Yarn Strain Sensor for Human Motion Tracking Utilizing a Wrinkle-Assisted Crack Structure. ACS Appl. Mater. Interfaces 2019, 11, 36052—36062.

- (29) Kim, M.; Kim, D. J.; Ha, D.; Kim, T. Cracking-assisted fabrication of nanoscale patterns for micro/nanotechnological applications. *Nanoscale* **2016**, *8*, 9461–9479.
- (30) Kim, H.; Jang, H.; Kim, B.; Kim, M. K.; Wie, D. S.; Lee, H. S.; Kim, D. R.; Lee, C. H. Flexible elastomer patch with vertical silicon nanoneedles for intracellular and intratissue nanoinjection of biomolecules. *Sci. Adv.* **2018**, *4*, No. eaau6972.
- (31) Zhu, X.; Mills, K. L.; Peters, P. R.; Bahng, J. H.; Liu, E. H.; Shim, J.; Naruse, K.; Csete, M. E.; Thouless, M. D.; Takayama, S. Fabrication of reconfigurable protein matrices by cracking. *Nat. Mater.* **2005**. *4*. 403–406.
- (32) Kim, M.; Kim, T. Crack-Photolithography for Membrane-Free Diffusion-Based Micro/Nanofluidic Devices. *Anal. Chem.* **2015**, *87*, 11215–11223.
- (33) Chung, S.; Lee, J. H.; Moon, M.-W.; Han, J.; Kamm, R. D. Non-Lithographic Wrinkle Nanochannels for Protein Preconcentration. *Adv. Mater.* **2008**, *20*, 3011–3016.
- (34) Kim, B. C.; Moraes, C.; Huang, J.; Matsuoka, T.; Thouless, M. D.; Takayama, S. Fracture-based fabrication of normally closed, adjustable, and fully reversible microscale fluidic channels. *Small* **2014**, *10*, 4020–4029.
- (35) Reeder, J. T.; Xue, Y.; Franklin, D.; Deng, Y.; Choi, J.; Prado, O.; Kim, R.; Liu, C.; Hanson, J.; Ciraldo, J.; Bandodkar, A. J.; Krishnan, S.; Johnson, A.; Patnaude, E.; Avila, R.; Huang, Y.; Rogers, J. A. Resettable skin interfaced microfluidic sweat collection devices with chemesthetic hydration feedback. *Nat. Commun.* **2019**, *10*, No. 5513.
- (36) Choi, J.; Kang, D.; Han, S.; Kim, S. B.; Rogers, J. A. Thin, Soft, Skin-Mounted Microfluidic Networks with Capillary Bursting Valves for Chrono-Sampling of Sweat. *Adv. Healthcare Mater.* **2017**, *6*, No. 1601355.
- (37) Guler, M. T.; Beyazkilic, P.; Elbuken, C. A versatile plug microvalve for microfluidic applications. *Sens. Actuators, A* **2017**, 265, 224–230.
- (38) Chen, Y.; Shen, M.; Zhu, Y.; Xu, Y. A novel electromagnet-triggered pillar valve and its application in immunoassay on a centrifugal platform. *Lab Chip* **2019**, *19*, 1728–1735.
- (39) Ouyang, M.; Yuan, C.; Muisener, R. J.; Boulares, A.; Koberstein, J. T. Conversion of Some Siloxane Polymers to Silicon Oxide by UV/Ozone Photochemical Processes. *Chem. Mater.* **2000**, 12, 1591–1596.
- (40) Efimenko, K.; Wallace, W. E.; Genzer, J. Surface Modification of Sylgard-184 Poly(dimethyl siloxane) Networks by Ultraviolet and Ultraviolet/Ozone Treatment. *J. Colloid Interface Sci.* **2002**, 254, 306–315
- (41) Fuard, D.; Tzvetkova-Chevolleau, T.; Decossas, S.; Tracqui, P.; Schiavone, P. Optimization of poly-di-methyl-siloxane (PDMS) substrates for studying cellular adhesion and motility. *Microelectron. Eng.* **2008**, 85, 1289–1293.
- (42) Mills, K. L.; Huh, D.; Takayama, S.; Thouless, M. D. Instantaneous fabrication of arrays of normally closed, adjustable, and reversible nanochannels by tunnel cracking. *Lab Chip* **2010**, *10*, 1627–1630.
- (43) Cho, H.; Kim, H. Y.; Kang, J. Y.; Kim, T. S. How the capillary burst microvalve works. *J. Colloid Interface Sci.* **200**7, *306*, 379–385.
- (44) Beebe, D. J.; Mensing, G. A.; Walker, G. M. Physics and Applications of Microfluidics in Biology. *Annu. Rev. Biomed. Eng.* **2002**, *4*, 261–286.